# Charge-Transfer Excited State Dynamics in DNA Hairpins Substituted with an Ethylenylpyrenyl-dU Electron Source and Halo-dU Traps

**Samir T. Gaballah,[†,§] Jonathan D. Vaught,[‡] Bruce E. Eaton,[‡] and Thomas L. Netzel*[,†]**

*Department of Chemistry, Georgia State University, P.O. Box 4098, Atlanta, Georgia 30302-4098, and Department of Chemistry, North Carolina State University, P.O. Box 8204, Raleigh, North Carolina 27695-8204*

*Received: November 3, 2004; In Final Form: January 19, 2005*

In this work nine DNA hairpins (HPs) are studied at room temperature to observe their pyrene$^{\bullet+}$/dU$^{\bullet-}$ CT excited-state dynamics following photoexcitation at 355 nm with a 25 ps laser pulse. The HPs are 18−24 bases long, have a central tetra-T loop, and have a single U$^{PE}$ (5-(2-pyren-1-yl-ethylenyl)-2′-deoxyuridine) substitution in the central region of their stems. Three of the HPs are also substituted with 5-XdU traps, where X = Br or F, to learn about the effects of these traps on CT excited-state lifetimes and emission quantum yields in U$^{PE}$ substituted HPs. The combination of lengthened average CT lifetime and enhanced CT emission quantum yield in HPs with excess electron traps compared to HPs lacking traps strongly suggests that excess electrons are injected into the DNA stem at pyrimidine sites external to U$^{PE}$ as well via charge separation within U$^{PE}$ itself. Furthermore, the increased CT emission quantum yield in HPs with traps compared to HPs without traps implies that externally injected electrons can migrate to uracil in U$^{PE}$ (i.e., Py$^{\bullet+}$dU) and thus indirectly form the emissive Py$^{\bullet+}$dU$^{\bullet-}$ CT state of U$^{PE}$.

## Introduction

Excess electron transfer (ET) or transport in DNA can occur if a covalently attached electron donor is photoexcited and injects one of its electrons into the DNA $\pi$-stack. In contrast to the heavily studied area of oxidative hole transfer and hopping in DNA,[1,2] the mechanistic details of excess electron transfer in DNA are still not well understood. Important initial investigations in this area were based on pulse radiolysis as a means of adding an excess electron to DNA.[3−8] Indeed, recently, seemingly contradictory results have been reported for excess electron-transfer processes in DNA, but the apparent differences could result from the different types of excess electron generation and detection in the reported experiments.[9−12] To date photochemical studies of electron injection and transport in DNA have employed flavine,[11,13−16] stilbene diether,[17−19] 1,5-diaminonaphthalene,[10,20] pyrene,[21−24] and ketyl radical anion[9] as excess electron sources.

Wagenknecht, Fiebig, and co-workers produced DNA duplexes substituted with two kinds of pyrenyl-dU nucleotide conjugates.[21−24] One type of pyrenyl-nucleotide was based on the 5-(pyren-1-yl)-2′-deoxyuridine (PdU) nucleoside originally prepared and studied by Netzel, Eaton, and co-workers.[25,26] In PdU the pyrenyl and uracil subunits were directly bonded together. The second type of pyrenyl-nucleotide conjugate was based on the 5-(pyren-1-yl-ethynyl)-2′-deoxyuridine nucleoside (PYdU) originally prepared by Korshun and co-workers.[27] In PYdU the pyrenyl and uracil subunits were joined by an ethynyl linker. It is clear from the above as well as from other spectroscopic studies of pyrenyl-dU nucleoside conjugates[28−31] that photoexcitation of the pyrenyl chromophore in these conjugates in a polar solvent initially forms the local pyrenyl $^1(\pi,\pi^*)$ excited state, but that this state in turn rapidly undergoes intramolecular ET to form the pyrene$^{\bullet+}$/dU$^{\bullet-}$ charge separated (CS) product. Both of these states emit, but the pyrenyl $^1(\pi,\pi^*)$ state emits at higher energy than the pyrene$^{\bullet+}$/dU$^{\bullet-}$ CS product and has three distinct, carbon−carbon stretching vibrational features. The emission spectrum of the pyrene$^{\bullet+}$/dU$^{\bullet-}$ CS (or charge transfer, CT) product, in contrast, is broad and structureless beginning in the pyrenyl $^1(\pi,\pi^*)$ emission region and extending over 100 nm beyond the pyrenyl region to lower energy.

In this work nine DNA hairpins (HPs) are studied at room temperature to observe their pyrene$^{\bullet+}$/dU$^{\bullet-}$ CT excited-state dynamics following photoexcitation at 355 nm with a 25 ps laser pulse. All of the HPs are 18−24 bases long, have a central tetra-T loop, and have a single U$^{PE}$ (5-(2-pyren-1-yl-ethylenyl)-2′-deoxyuridine) substitution in the central region of their stems. (See Chart 1 for a schematic drawing of a representative HP and a structural drawing of the U$^{PE}$ nucleotide). Importantly, measurement of the kinetics of CT emission in the red, beyond the pyrenyl emission range, allows direct observation of the lifetime of the Py$^{\bullet+}$/dU$^{\bullet-}$ CT state within U$^{PE}$.

Chart 1 describes in schematic form various charge separation (CS), excess electron transfer ($e^-$-hops), and charge recombination (CR) processes that, in principle, can occur in a U$^{PE}$ substituted HP following photoexcitation. Importantly, for this study some HPs are substituted with U$^X$, where X = Br or F, excess electron traps on the same strand as U$^{PE}$ in the 5′-direction, while others lack such traps. Photoexcitation at 355 nm or below initially produces the pyrenyl $^1(\pi,\pi^*)$ state in a U$^{PE}$ substituted HP (see panel a). This excited state can be oxidatively quenched by nearby T, C, and U pyrimidine bases either within U$^{PE}$ itself (CS-1 type quenching) or external to U$^{PE}$ (CS-2 type quenching). In principle, an excess electron on uracil in U$^{PE}$ can hop to neighboring pyrimidines either on the

† Georgia State University.
‡ North Carolina State University.
* Corresponding author. E-mail: tnetzel@gsu.edu.
§ Current address: Department of Photochemistry, National Research Center, El Tahrir Street, Dokki, Cairo, Egypt.

10.1021/jp044968j CCC: $30.25 
Published on Web 03/02/2005

**CHART 1**[a]

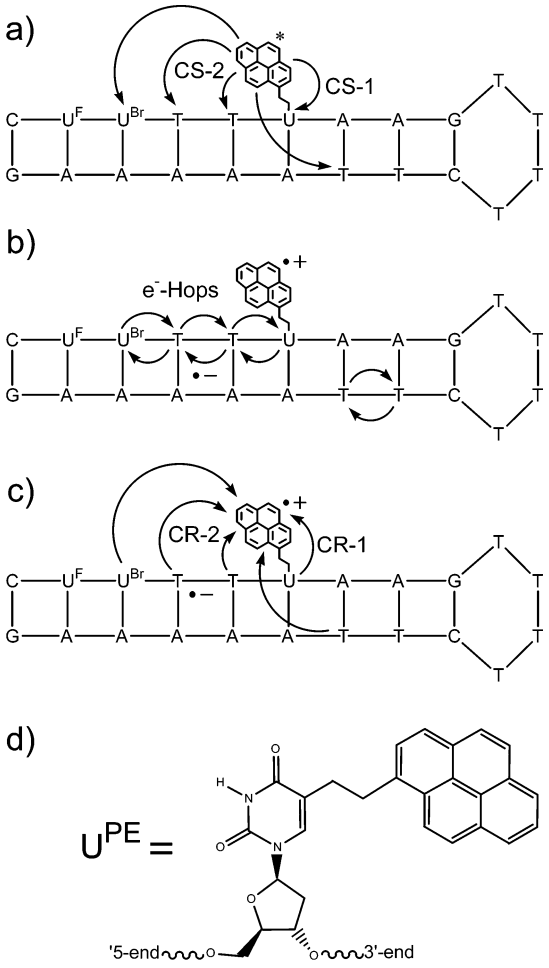


[a] Panels a−c are schematic drawings of some possible charge separation (CS), excess electron transfer ($e^-$-hops), and charge recombination (CR) reactions in DNA hairpin **8** (see Table 1 for hairpin numbering). $U^{Br}$ and $U^F$ are excess electron traps, respectively, 5-bromo- and 5-fluoro-2′-deoxyuridine. The $*$ symbol in panel a indicates the initially excited, emissive $^1(\pi,\pi^*)$ state of the pyrenyl chromophore. The $^{\bullet+}$ symbol indicates the pyrenyl cation, while the $^{\bullet-}$ symbol indicates an excess electron that can potentially reside on any pyrimidine base in **8** both external to or within $U^{PE}$. Two types of CS and CR electron transfer reactions are distinguished in the chart: Type 1 reactions occur internally within the $U^{PE}$ nucleotide, while type 2 reactions occur between the pyrenyl chromophore of $U^{PE}$ and external bases. Note that the product of the CS-1 reaction from $U^{PE*}$ is the emissive $Py^{\bullet+}/dU^{\bullet-}$ CT excited state of $U^{PE}$. Panel d is a structural drawing of the C5-substituted 2′-deoxyribonucleotide, $U^{PE}$.

same stem-strand or on the opposite stem-strand (see panel b). Also, an excess electron on a pyrimidine near $U^{PE}$ (perhaps formed via CS-2 type ET) can hop to neighboring pyrimidines, including uracil in $U^{PE}$. In the latter case, the emissive $Py^{\bullet+}/dU^{\bullet-}$ CT state within $U^{PE}$ would be formed. Finally, panel c shows that excess electrons on pyrimidines in HPs can recombine with $Py^{\bullet+}$ in $U^{PE}$ ($Py^{\bullet+}dU$) either within the $Py^{\bullet+}/dU^{\bullet-}$ CT state of $U^{PE}$ (CR-1 type recombination) or directly between excess electrons on bases external to $U^{PE}$ and $Py^{\bullet+}dU$ (CR-2 type recombination).

The studies of $Py^{\bullet+}/dU^{\bullet-}$ CT excited-state dynamics in $U^{PE}$ substituted HPs presented here seek to learn about the effects of locating same-strand, flanking pyrimidines on either side of $U^{PE}$, the effects of $U^X$ traps on CT excited-state lifetimes and emission quantum yields, whether CS-2 type processes are important, and if so, can excess electron transport to $Py^{\bullet+}dU$ compete with direct CR-2 type recombination processes. Some idea of the relative effect on uracil reduction potential due to changing the C5-methyl in T to F or Br can be estimated by noting that in the case of flavin mononucleotide (FMN) the $2e^-$ reduction potential of $FMN_{ox}$/1,5-dihydro-$FMN_{red}H_2$ varies due to substitution at position 8, respectively, as −208 (Me), −167 (F), and −148 (Br) vs the standard hydrogen electrode.[32] Alternately, adiabatic electron affinities calculated using density functional theory (DFT) give a similar ordering of the ease of reducing, respectively, uracil, 5-fluorouracil, and 5-bromouracil as 0.18 eV (gas)/2.02 eV (solvated), 0.48 eV (gas)/2.21 eV-(solvated), and 0.63 eV(gas)/2.44 eV(solvated).[33] Thus, $U^X$ nucleotides are expected to be easier to reduce than U or T with $U^{Br}$ a slightly better excess electron trap than $U^F$. Whether or not $U^X$ nucleotides will be deep enough traps to inhibit excess electrons on them from hopping to neighboring pyrimidines is an open question.

## Experimental Materials and Methods

**Materials**. Chemicals were purchased from the indicated vendors and used as received: monobasic sodium phosphate monohydrate ($NaH_2PO_4{\cdot}H_2O$, J. T. Baker), ethylenediaminetetraacetic acid disodium salt ($Na_2EDTA$, Fisher Scientific Co.), and sodium chloride (Aldrich Chemicals). Solvents and samples for spectroscopy were purchased from the following vendors and used as received: pyrenebutanoic acid (PBA, high purity grade) from Molecular Probes; and methanol (MeOH), acetonitrile (MeCN), and tetrahydrofuran (THF) were purchased from Burdick & Jackson (spectroscopic or HPLC grade). Deionized water (18.0 MΩ) was obtained from a Milli-Q Plus system (Millipore). To make 7.5 mM phosphate buffer solution, $NaH_2PO_4{\cdot}H_2O$ (1.035 g) and $Na_2EDTA$ (0.375 g) were added to a 1-L volumetric flask and dissolved in deionized water. The final pH was adjusted to $7.0 \pm 0.1$ using a pH meter (JENCO model 6071). This phosphate buffer solution was used to make the 1.0 M NaCl buffer solution used in spectroscopic studies.

**DNA Hairpin Synthesis.** DNA 18-mer single strands (see Chart 1) were synthesized at North Carolina State University using a $U^{PE}$ $\beta$-cyanoethylphosphoramidite synthesized at either North Carolina State University or Georgia State University. Standard solid-phase DNA synthetic protocols were followed using an ABI 394 (Applied Biosystems) DNA synthesizer. All strands were synthesized in 1 $\mu$mol batches. Lyophilized strands were dissolved in a PTFE vial in 1 mL of DI water from a Millipore Milli-Q system, wrapped in aluminum foil, and stored in a freezer for future use.

**DNA Purification and Desalting.** DNA samples were purified on a Varian ProStar HPLC equipped with a reverse-phase column (PRP-1) heated to 70 °C (10−50% gradient of a 1:1 ratio of 0.01 M ethylenediamonium acetate (pH 7.6) and acetonitrile in neat 0.01 M ethylenediamonium acetate (pH 7.6). Collected 1.5 mL fractions were immediately evaporated using a Speed-Vac and pooled as a 1 mL sample in a 2 mL PTFE vial using a syringe. Purified oligomers were desalted using disposable, Pharmacia Sephadex G-25 desalting columns and a 1:1 mixture of acetonitrile and water. Desalted strands were freeze-dried and then hydrated and annealed as follows: $U^{PE}$-substituted DNA hairpins ($A_{260} = 4.8$) were dissolved in 250 $\mu$L of Milli-Q deionized water in a 1 mL Eppendorf tube. This solution of DNA was heated to 90 °C, maintained at that temperature for 2 min, and then allowed to cool to room temperature. Annealed stock solutions of hairpins were stored in a freezer at −20 °C for future use. Measured aliquots of the stock HP solution in deionized water were added to our standard

**TABLE 1: DNA Hairpin Sequence, Melting Temperature ($T_m$), and Emission Quantum Yield ($\Phi_{Em}$)**

| HP | base sequence[a] | no. of bases | $T_m$ (°C) | $\Phi_{em}$ ($\times 10^2$)[b] |
|---|---|---|---|---|
| **1** | TT**U**$^{PE}$TTTG TTTT AAAAAAA | 18 | 54.1 ± 0.5 | 0.16 |
| **2** | CTT**U**$^{PE}$TTG TTTT AAAAAAG | 18 | 57.1 ± 1.0 | 0.23 |
| **3** | GTT**U**$^{PE}$TTG TTTT AAAAAAC | 18 | 58.4 ± 0.4 | 0.14 |
| **4** | TTTTTT**U**$^{PE}$AAG TTTT CTTAAAAAAA | 24 | 66.4 ± 0.3 | 0.40 |
| **5** | GAA**U**$^{PE}$AAG TTTT ATTATTC | 18 | 51.0 ± 0.3 | 0.75 |
| **6** | CTU$^{F}$**U**$^{PE}$AAG TTTT CTTAAAG | 18 | 57.2 ± 0.7 | 1.04 |
| **7** | CTU$^{F}$U$^{Br}$**U**$^{PE}$AAG TTTT CTTAAAAG | 20 | 57.5 ± 0.3 | 0.64 |
| **8** | CU$^{F}$U$^{Br}$TT**U**$^{PE}$AAG TTTT CTTAAAAAG | 22 | 60.6 ± 0.3 | 1.21 |
| **9** | TTT**U**$^{PE}$TTG TTTT AAAAAAA | 18 | 52.7 ± 0.5 | 0.27 |

[a] 5′→3′ base sequence. [b] Emission quantum yields were measured relative to PBA in deaerated MeOH with $\Phi_{em}$ equal to 0.065.[26] $\Phi_{em}$ errors are ±10%.

buffer (7.5 mM phosphate buffer at pH 7.0 with 10 $\mu$M $Na_2$-EDTA and 1.0 M NaCl) for absorbance and $T_m$ measurements. Salt-free samples were submitted for mass spectral analysis.

**DNA Hairpin Analysis.** Mass spectra were run on all oligomers at the Georgia Institute of Technology using electrospray ionization (ESI). Found masses of all hairpins were within 0.7 (average deviation ±0.4) mass units of the calculated value (i.e., ±1.2 parts per 10 000). Hairpin melting ($T_m$) experiments were run on a Varian Carey 3E UV−vis spectrophotometer equipped with a Cary temperature controller. The absorbance was measured at 260 nm between 10 and 95 °C using a 0.5 °C/min temperature gradient. $T_m$ values from heating and cooling cycles for each sample agreed within ±0.05 °C. Hairpin concentrations for $T_m$ measurements ranged from 2 to $4 \times 10^{-6}$ M.

**Concentration of DNA Hairpins.** We assumed that the integrated molar absorbance of PEdU (the nucleoside form of $U^{PE}$) in the strongly allowed $S_2$ excited-state region from 290 to 360 nm in MeOH was the same as that of $U^{PE}$ labeled hairpins in the 310−375 nm region in buffer. Thus, a known concentration of PEdU based on sample weight in a known volume was related to an unknown concentration of hairpin. The resulting concentration of hairpin (HP) yielded a duplex molar absorbance at 351 nm in buffer of 33 000 ± 2000 $M^{-1}$ $cm^{-1}$.

**UV—Vis and Circular Dichroism (CD) Absorbance.** UV−vis absorbance spectra were recorded on a Shimadzu UV-2501PC high performance spectrophotometer equipped with a double monochromator to reduce stray light. CD absorbance spectra were recorded on a JASCO-810 spectropolarimeter using a 1 nm spectral bandwidth (SBW) and self-masking semimicro quartz cells. Absorbances of hairpin solutions at 260 nm were adjusted to 0.8−0.9. CD spectra were recorded in the 205−400 nm range at a scan speed of 50 nm/min, and six scans were averaged for each spectrum. The CD spectra of identical buffer solutions lacking DNA hairpins were used to correct the baseline of the CD spectra of DNA solutions.

**Emission Spectra and Emission Quantum Yield Measurements**. Quartz fluorescence cuvettes with open-screw caps and Teflon-silicone septa (Wilmad Glass, WG-9F/OC-Q-10) were used for steady-state emission spectra and emission lifetime studies (see below). All samples, except those used for UV−vis and CD absorbance, were deoxygenated by bubbling the sample solutions with water-saturated $N_2$ gas for 30−40 min inside of their quartz cells. Hairpin concentrations for emission spectra and quantum yield measurements were $(3-5) \times 10^{-6}$ M. Emission spectra were recorded on PTI QuantaMaster spectrofluorometer using 3 nm excitation and 2 nm emission spectral bandwidths. Samples were excited at 341 nm in a quartz 1 cm path length cuvette using right-angle excitation and emission geometry. Polarization artifacts were avoided by positioning a vertical polarizer immediately in front of the sample in the excitation beam and recording emission spectra through a second polarizer adjusted to 54.7° with respect to vertical ("magic angle"). All spectra were corrected for the wavelength-dependent emission sensitivity of the spectrofluorometer (W/cm$^2$ units) using correction factors developed at GSU. Details for emission quantum yield ($\Phi_{em}$) measurements are provided in the Supporting Information (SI) material and in Table 1.

**Picosecond Emission Lifetime Measurements.** Emission lifetime measurements were carried out using third harmonic pulses (355 nm) from a custom-built picosecond laser flash-photolysis system as the excitation source.[34,35] In this system, an active-passive mode-locked, Q-switched $Nd^{3+}$/YAG laser (Continuum, Inc.) was operated at 15 Hz to produce single excitation pulses of ~35 $\mu$J of energy with durations of ca. 25 ps (fwhm). The excitation beam was collimated to 3 mm diameter at the emission cell and passed through a Glan-Thompson laser polarizer set to vertical prior to entering the sample cell. The excitation and emission beams were oriented at 90° with respect to each other. Emission was detected through a second Glan-Thompson polarizer set at 54.7° with respect to vertical ("magic angle")[36] and was resolved by a double monochromator (Instruments SA, Inc. model DH10) in additive dispersion; 2 mm slits were used producing an 8 nm SBW. The monochromator's output was detected by a Hamamatsu R1564U microchannel plate (MCP, 200 ps rise time) for short emission lifetimes (≤50 ns digitization window) or a Hamamatsu R928 photomultiplier (2.2 ns rise time) for long ones (>50 ns digitization window). The detector response was recorded by a Tektronix SCD1000 transient digitizer (≤0.35 ns rise time calculated from the bandwidth, ≤120 ps rise time for a step input 0.5 times the vertical range). Each transient measurement, whether of a sample's emission decay, the instrument response to scattered laser light, or the detector's background, was recorded as a 500-point average of 1000 laser firings. Additional details of the lifetime fitting procedure that was used in this study are given in the SI material and a complete description has been presented by Netzel et al.[26] UV−vis absorbance spectra of each sample solution were measured before and after emission lifetime measurements to verify that no decomposition occurred during the course of these measurements.

Emission lifetimes from multiexponential fits to emission decay kinetics at individual wavelengths are given in Table 1S for all nine HPs studied along with sample concentration ($1.0-2.5 \times 10^{-5}$ M range) and cell geometry information. The amplitude-weighted average emission lifetime, $\langle\tau\rangle$, at each wavelength is also given in Table 1S. In Table 2, $\langle\tau\rangle$ and $\langle\tau\rangle^{525}$ are lifetime averages over specified wavelength regions, respectively, the amplitude weighted average of wavelength-averaged lifetime components and amplitudes and linear least squares fit values at 525 nm of single-wavelength average

**TABLE 2: Wavelength Averaged Kinetics Data for Nine Hairpins at Room Temperature[a,b]**

Dual Emission

| hairpin | wavelength range (nm)[c] | $\langle\tau_1\rangle$, ns ($A_1$) | $\langle\tau_2\rangle$, ns ($A_2$) | $\langle\tau_3\rangle$, ns ($A_3$) | $\langle\tau_4\rangle$, ns ($A_3$) | $\langle\tau\rangle$, ns[d] |
|---|---|---|---|---|---|---|
| **1** | 380−450 | 0.07 (0.61) | 0.46 (0.23) | 2.41 (0.12) | 8.17 (0.04) | 0.75 ± 0.05 |
| **2** | 380−450 | 0.10 (0.56) | 0.42 (0.27) | 2.06 (0.11) | 8.93 (0.06) | 0.93 ± 0.20 |
| **3** | 380−475 | 0.08 (0.60) | 0.44 (0.31) | 2.22 (0.06) | 9.62 (0.03) | 0.65 ± 0.04 |
| **4** | 380−425 | 0.09 (0.69) | 0.52 (0.19) | 1.74 (0.09) | 9.57 (0.03) | 0.58 ± 0.11 |
| **5** | 425−475 | 0.06 (0.31) | 0.46 (0.30) | 1.47 (0.29) | 7.70 (0.10) | 1.36 ± 0.30 |
| **6** | n.a. | n.a. | n.a. | n.a. | n.a. | n.a. |
| **7** | 380−400 | 0.08 (0.75) | 0.53 (0.14) | 2.27 (0.08) | 8.57 (0.04) | 0.61 ± 0.02 |
| **8** | 380−475 | 0.12 (0.58) | 1.02 (0.20) | 2.78 (0.17) | 8.90 (0.05) | 1.19 ± 0.35 |
| **9** | 380−425 | 0.17 (0.36) | 0.44 (0.38) | 2.36 (0.17) | 9.68 (0.09) | 1.47 ± 0.55 |

CT Emission

| hairpin | wavelength range (nm)[c] | $\langle\tau_2\rangle$, ns ($A_1$) | $\langle\tau_3\rangle$, ns ($A_2$) | $\langle\tau_4\rangle$, ns ($A_3$) | $\langle\tau\rangle^{525}$, ns[e] | $R$[f] |
|---|---|---|---|---|---|---|
| **1** | 475−550 | 0.31 (0.74) | 2.00 (0.18) | 7.95 (0.08) | 1.16 | 0.99 |
| **2** | 475−550 | 0.36 (0.76) | 1.84 (0.16) | 7.71 (0.08) | 1.07 | 0.93 |
| **3** | 500−550 | 0.34 (0.83) | 1.53 (0.12) | 7.87 (0.05) | 0.85 | 1.00 |
| **4** | 500−550 | 0.35 (0.68) | 1.41 (0.27) | 8.07 (0.05) | 0.99 | 1.00 |
| **5** | 500−550 | 0.24 (0.44) | 1.14 (0.48) | 6.93 (0.08) | 1.22 | 1.00 |
| **6** | 475−550 | 0.30 (0.61) | 2.02 (0.17) | 8.28 (0.22) | 2.07 | 1.00 |
| **7** | 475−550 | 0.43 (0.57) | 2.27 (0.24) | 8.15 (0.19) | 2.10 | 0.97 |
| **8** | 500−550 | 0.77 (0.48) | 2.41 (0.37) | 8.60 (0.15) | 2.52 | 0.91 |
| **9** | 450−500 | 0.49 (0.61) | 2.81 (0.21) | 7.78 (0.18) | 2.30[g] | n.a. |

[a] Samples were dissolved in 7.5 mM phosphate buffer at pH 7.0 with 10 $\mu$M $Na_2EDTA$ and 1.0 M NaCl. For HPs **1**−**3** and **9** sample concentrations were (2.1−2.5) × $10^{-5}$ M, and $A_{355}$ in a 1 cm path length cell ranged from 0.47 to 0.67. For HPs **4**−**8,** sample concentrations were (1.0−1.2) × $10^{-5}$ M, and $A_{355}$ in a 1 cm path length cell ranged from 0.26 to 0.36. $\lambda_{exc}$ was 355 nm. Samples were held in quartz semimicro cells and excited through the 4 mm path length. All samples were deoxygenated prior to kinetics measurements by bubbling with $N_2$ gas while stirring for 30−40 min. Spectral bandwidth for emission measurements was 8 nm. [b] Emission decay lifetimes were fit to $f(t) = \sum_{i=1}^{n} A_i e^{-t/\tau_i}$, *where* $n = 3$ *or* 4. Residuals in the fits ranged from 3 to 10, and reduced $\chi^2$ values for the fits ranged from 1 to 14. [c] Emission component lifetimes and amplitudes averaged over the indicated wavelength ranges. [d] Average lifetime, $\langle\tau\rangle = \sum_{i=1}^{n} A_i\tau_i$, *where* $n = 3$ *or* 4. Errors are the standard deviations of the average lifetime at each wavelength in the range. [e] Characteristic average lifetime at 525 nm from a linear least squares fit of average lifetime vs energy over the specified wavelength range. Errors are equal to ±0.15 ns unless specified otherwise. [f] Linear correlation coefficient ($R$) for the fit of lifetime vs energy. [g] Average over the specified wavelength range of the average lifetime at each wavelength in the range. Error is the standard deviation of the average lifetime at each wavelength, ±0.20 ns.

lifetimes plotted as a function of emission energy. Table 2 also lists and defines error values for the $\langle\tau\rangle$ and $\langle\tau\rangle^{525}$ emission lifetime averages over specified wavelengths for all nine $U^{PE}$-substituted DNA hairpins.

## Results and Discussion

**DNA Hairpin Sequences.** Chart 1 presents a schematic drawing of HP **8** with the $U^{PE}$ photoelectron source and both $U^{Br}$ and $U^{F}$ excess electron trap nucleotides, and Chart 2 presents a molecular model of the same HP. Table 1 lists the base sequence, number of bases, melting temperature, and emission quantum yield for each of the nine HPs in this study. All of the HPs in Table 1 have a common tetra-T loop with the photoelectron source $U^{PE}$ substituted in the stem's 5′-strand two or three bases from the loop. The number of bases in the nine HPs varies from 18 to 24, while the melting temperatures ($T_m$s) range from 51 to 66 °C. Generally the longer length HPs melt at higher temperatures than the shorter ones (57−66 °C for 20−24 bases vs 51−58 °C for 18 bases). Inspection of the melting curves for these nine HPs shows that they all begin to melt above room temperature, and thus all spectroscopic studies reported here were carried out at room temperature where their stem structures are intact. Review of published DNA and RNA loop structures[37,38] suggests that choice of G:C or G:A as a loop-closing base pair for a tetra-T DNA loop will not affect HP structure. Our, largely historical, reasons for using both types of loop-closing bases in this study are given in a ref 39.

The HPs in Table 1 fall into two main groups: those containing $U^{F}$ and $U^{Br}$ excess electron traps (**6**−**8**) and those lacking electron traps (**1**−**5** and **9**). It can also be seen from the emission quantum yield data in Table 1 that the lowest emission quantum yields [(0.14−0.27) × $10^{-2}$] belong to HPs **1**−**3** and **9** all of which lack traps, while larger emission quantum yields

**CHART 2: Molecular Mechanics Model[a] of HP 8 Built with HyperChem 7.51 Using the Amber99 Force Field[40]**

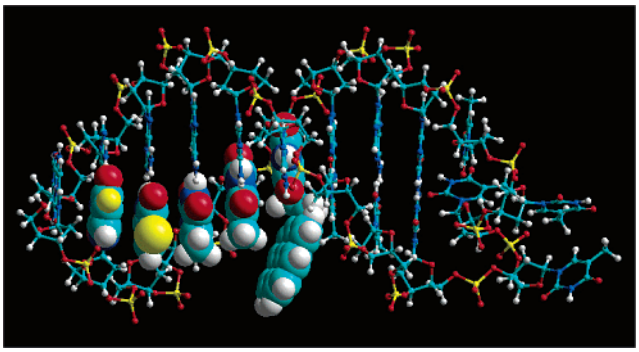

[a] The backbone and base pairs in the stem were constrained to B-form DNA geometry, while all modifications at C5-uracil positions and the tetra-T loop were simultaneously geometry optimized. (Other energy-minimized conformations with different pyrenyl and loop geometries also exist.) In place of explicit solvent and counterions, a distance-dependent dielectic constant of 78 was used with no cutoff for nonbonded interactions. In the chart the tetra-T loop is on the right, and the HP's stem is on the left. Five same-strand uracils in the stem are shown as overlapping spheres of van derWaals radius, 5′-$U^{F}U^{Br}TTU^{PE}$-3′; their C5-substituents, respectively, F, Br, Me, Me, and ethylenylpyrenyl are turned toward the reader. The rest of the HP is displayed as a balls-and-cylinders rendering.

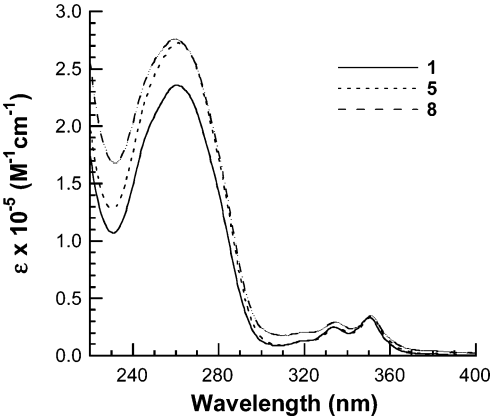


**Figure 1.** Overlayed molar absorbance plots in the 220−400 nm wavelength range for three DNA HPs each in 7.5 M phosphate buffer at pH 7.0 with 10 $\mu$M $Na_2EDTA$ and 1.0 M NaCl.

[(0.64−1.21) × $10^{-2}$] belong to HPs **6**−**8** all of which contain traps. HPs **4** and **5** have intermediate emission quantum yields, respectively, 0.40 and 0.75 × $10^{-2}$, but their emission spectra differ from those of the other seven HPs in that they have significantly more pyrenyl $^1(\pi,\pi^*)$ emission (see Figure 2 below). Pyrene butanoic acid (PBA) has an emission quantum yield of 0.065 and an emission lifetime in deoxygenated MeOH of ca. 100 ns.[26] These data imply a radiative lifetime of ca. 1.5 $\mu$s for the orbitally forbidden, lowest energy $^1(\pi,\pi^*)$ state of PBA. The lowest energy $Py^{\bullet+}/dU^{\bullet-}$ $^1$CT state of $U^{PE}$ is optically forbidden also, because it too shows almost no electronic absorbance (see Figure 1). Assuming for the sake of argument that the $^1$CT state of $U^{PE}$ also has a 1.5 $\mu$s radiative lifetime, one can calculate an expected emission lifetime for this state from the emission quantum yield data in Table 1. For example, an emission quantum yield of ca. 0.2 × $10^{-2}$ (like those of HPs **1**−**3** in Table 1) suggests that the observed emission lifetime for the $^1$CT state of $U^{PE}$ in these HPs should be ca. 3 ns (i.e., a few ns). Table 2 below shows that they have average CT emission lifetimes of ca. 1 ns. Thus, there are three reasons for the low emission quantum yields in Table 1: (1) the pyrenyl $^1(\pi,\pi^*)$ state is nearly completely quenched due to ET within these HPs; (2) the optically forbidden, $^1$CT state of $U^{PE}$ has a low radiative rate; (3) the $^1$CT state's lifetime is shortened in these HPs to ca. 1 ns on average due to rapid CR processes.

**UV—Vis Absorbance and Circular Dichroism (CD) Spectra.** Figure 1 presents overlay plots of the molar absorbance ($\epsilon$) spectra for three representative HPs (**1**, **5**, and **8**) in phosphate buffer at pH 7.0. Molar absorbance spectra for the other six duplexes in this study are given in Figure 1S. Note that three C−C stretching bands of the pyrenyl subunit's $S_2$ electronic state are visible in the 310−375 nm region well above the wavelengths where the DNA bases absorb ($\lambda$ < 300 nm).

The CD spectra for all nine HPs are given in Figure 2S. All show characteristic B-form DNA CD signatures. Only one HP, **5**, shows noteworthy negative pyrenyl CD absorbance features in the 310−375 nm region. The absence of pyrenyl CD absorbance demonstrates that the pyrenyl chromophore of $U^{PE}$ is not located in a chiral environment as it would be, for instance, if it were intercalated between DNA bases. Its presence as in the case of **5** shows that the pyrenyl chromophore is held chirally somehow. It may be intercalated, but this is not necessarily true. Usually, intercalation of an attached chromophore such as pyrene leads to a higher $T_m$ value for a DNA duplex (or HP) compared to similar ones that do not have an intercalated chromophore. Yet, the data in Table 1 show that **5** has the lowest $T_m$ of the

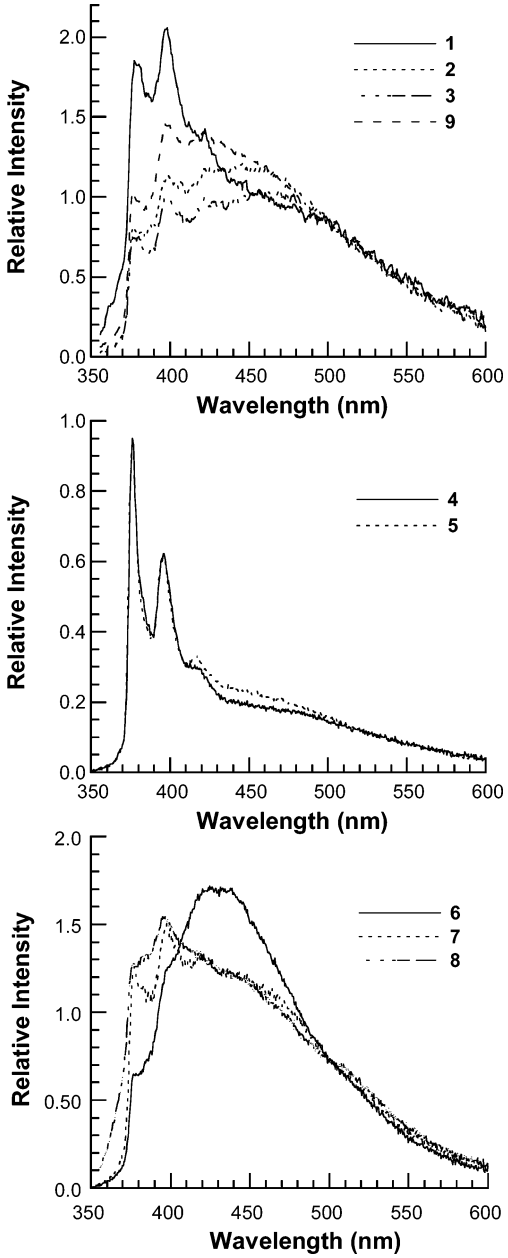


**Figure 2.** Overlayed plots of relative emission spectra for nine DNA hairpins in deoxygenated 7.5 mM phosphate buffer at pH 7.0 with 10 $\mu$M $Na_2EDTA$ and 1.0 M NaCl normalized to overlap at 500 nm in each plot. Hairpin concentrations were (3−5) × $10^{-6}$ M.

six HPs with 18 bases each. From a gross perspective all nine HPs in Table 1 have high $T_m$ values, reasonably similar UV−vis absorbance spectra, and B-form DNA CD signatures.

**Emission Spectra and Kinetics.** Figure 2 presents relative emission spectra for the nine HPs in Table 1. In each plot the overlayed spectra are normalized to overlap at 500 nm for relative shape comparisons. The emission spectra can be separated into two distinct groups. The first group contains HPs **1**−**3** and **6**−**9** as all seven have only hints of pyrenyl $^1(\pi,\pi^*)$ emission features at 376, 396, and 422 nm. Rather their spectra are almost entirely due to $Py^{\bullet+}/dU^{\bullet-}$ CT emission within the $U^{PE}$ nucleotide. This CT emission maximizes around 450 nm and extends far to the red of the pyrenyl emission, even beyond 600 nm. As expected for such emission, it is structureless due to strong coupling between the nuclear motions of the polar CT excited state and the buffer solution. Importantly, measurement of the CT emission kinetics to the red of the pyrenyl

emission range allows direct observation of the lifetime of the $Py^{\bullet+}/dU^{\bullet-}$ CT state within $U^{PE}$. The second HP spectral group has two members, **4** and **5**. In these two HPs, the pyrenyl $^1(\pi,\pi^*)$ emission features at 376, 396, and 422 nm dominate the $Py^{\bullet+}/dU^{\bullet-}$ CT emission from $U^{PE}$. This is a surprising result in each case as T, C and G nucleotides can all ET quench the pyrenyl $^1(\pi,\pi^*)$ excited state. HP **5** is surprising, because it has the same base content as **3**, except the two TT pairs flanking $U^{PE}$ in **3** are switched to the opposite stem-strand in **5**. HP **4** is surprising, because its base sequence near $U^{PE}$ is reasonably similar to that of **8** both having the same base sequence between $U^{PE}$ and the tetra-T loop and a string of five or six pyrimidines on the same stem-strand in the 5′-direction from $U^{PE}$. Nevertheless, pyrenyl $^1(\pi,\pi^*)$ emission from **8** is nearly absent, while it dominates CT emission in **4**. Clearly, the local environments surrounding $U^{PE}$ in **4** and **5** are distinctly different from the local environments surrounding $U^{PE}$ in the other seven HPs in Figure 2.

By considering the set of six HPs lacking $U^X$ electron traps (**1**−**5** and **9**), a pattern of emission spectral-type and quantum yield can be seen. HPs **1**−**3** have two or three Ts flanking $U^{PE}$ on the same stem-strand on both sides. They also have low emission quantum yields ($(0.14-0.23) \times 10^{-2}$) and CT emission band shapes with essentially complete quenching of pyrenyl $^1(\pi,\pi^*)$ emission. HP **4** in contrast has six Ts flanking $U^{PE}$ on the same stem-strand in the 5′-direction, but no same stem-strand pyrimidines in the 3′-direction. It has both a higher emission quantum yield ($0.40 \times 10^{-2}$) than HPs **1**−**3** and a large amount of pyrenyl $^1(\pi,\pi^*)$ emission. Clearly HPs **1**−**3** quench pyrenyl $^1(\pi,\pi^*)$ emission more effectively than does HP **4**. HP **5** confirms this explanation. HP **5** has no same stem-strand pyrimidines on either side of $U^{PE}$, and it has both a large amount of pyrenyl $^1(\pi,\pi^*)$ emission and the largest emission quantum yield of all six duplexes that lack $U^X$ traps, $0.75 \times 10^{-2}$. Thus, there is a pattern of increased emission quantum yield and lessening of pyrenyl $^1(\pi,\pi^*)$ emission quenching as same stem-strand pyrimidines flanking $U^{PE}$ are reduced from pyrimidines on both sides, to pyrimidines on only the 5′-side, to no pyrimidines on neither side of $U^{PE}$.

For each HP in this study, we measured the emission kinetics at eight wavelengths in the 380−500 nm range. In the blue, dual-emission region (containing both pyrenyl $^1(\pi,\pi^*)$ and CT emission) four exponential decay lifetimes were usually required to fit the emission kinetics; in the CT emission region three exponential decay lifetimes were always required. All of the lifetime fits for all of the HPs are presented in Table 1S. However, averaging the emission lifetimes and their corresponding amplitudes over each of the two emission regions condenses this information and makes it more useful for HP comparisons. These regionally averaged lifetime and amplitude components and their resulting average emission lifetime for each HP in each emission region are given in Table 2 along with the wavelength range for each type of emission.

A few observations based on the individual wavelength data in Table 1S are, however, worth making as they provide some interesting insights into the excited-state photochemistry of $U^{PE}$ labeled DNA duplex structures. All HPs except **6** show large amplitude (0.50−0.75), ultrashort $^1(\pi,\pi^*)$ emission decays with lifetimes of ca. 0.1 ns. These lifetimes are at the limit of the time resolution of our emission kinetics equipment, and thus faster decays may also be present and the amplitudes recorded for the ca. 0.1 ns decays may be underestimated. Nevertheless, these ultrashort $^1(\pi,\pi^*)$ emission decays clearly reflect the time scale of the dominant pyrenyl $^1(\pi,\pi^*)$ quenching and associated CS processes (whether type CS-1 or CS-2 cannot be determined). At long times (ca. 10 ns), the longest emission decays in the dual wavelength region generally exceed the lifetimes of the longest emission decays in the CT region. However, whether this effect is due to long-lived pyrenyl $^1(\pi,\pi^*)$ states or CT states is not clear. Both possibilities are reasonable. In contrast the shortest lifetimes for emission decay in the CT region are 0.3−0.5 ns for eight HPs and ca. 0.7 ns for HP **8**. One would expect some CT emission to grow in on the same time scale as the fastest pyrenyl $^1(\pi,\pi^*)$ quenching, but in these studies both the fastest pyrenyl quenching times and the fastest CT emission formation times are at the time resolution limit of our kinetics equipment. For this reason we made no attempt to fit the CT emission kinetics with a rising exponential lifetime component as we judged it difficult to separate a rising exponential lifetime from the rise of emission due to the convolution of the excitation pulse and the rise time of our detection electronics. However, the measurably longer shortest-emission lifetimes for CT emission for all nine HPs compared to the corresponding shortest-emission lifetimes in the dual wavelength region are convincing evidence for different photochemical processes occurring in each case: CS due to pyrenyl $^1(\pi,\pi^*)$ ET quenching in the dual wavelength region and CR of the $Py^{\bullet+}dU^{\bullet-}$ ET product in the CT region.

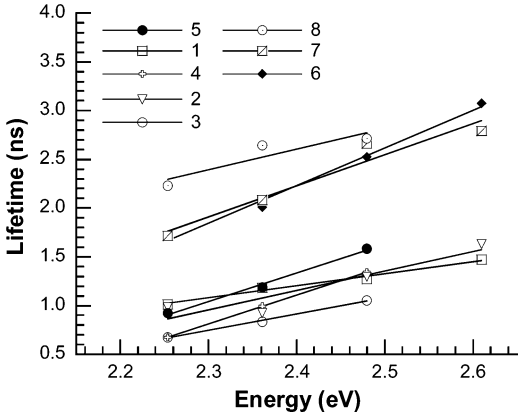


**Figure 3.** Overlayed plots of average CT emission lifetime vs energy (475−550 nm wavelength range) for eight DNA hairpins at room temperature. The experimental conditions are the same as those described in Table 2. The solid lines are linear least squares fits to the data. Linear Correlation Coefficients (R) for these fits are given in Table 2 for each HP.

The large amplitudes of the ultrashort $^1(\pi,\pi^*)$ emission decays in the dual wavelength region have the not surprising effect of causing an increase of the average emission lifetime as wavelength increases from 380 to 475 nm. That is, as the pyrenyl $^1(\pi,\pi^*)$ emission dies out as one approaches 475 nm from shorter wavelengths, the average emission lifetime increasingly reflects the average CT emission lifetime that does not have an ultrashort ca. 0.1 ns lifetime component. A completely unexpected observation can be seen in the average emission lifetime data in Table 1S in the CT region for all of the duplexes except **9**. In this region, the average CT emission lifetimes decrease as the wavelength increases from 475 to 550 nm; this is the opposite of the emission lifetime behavior seen in the blue, dual wavelength region. Figure 3 presents overlayed plots of the average CT emission lifetime vs emission energy for HPs **1**−**8**. The linear correlation coefficients (*R*) for each of these fits are given in Table 2; they range from 0.91 to 1.00.

One result that is apparent in the lifetime vs energy plots of Figure 3 is that the three HPs with $U^X$ excess electron traps (**6**−**8**) have longer CT emission lifetimes at all wavelengths than five of the HPs that lack electron traps (**1**−**5**). Compared

to the other HPs that lack electron traps, HP **9** is anomalous. First, it is the only HP of the nine studied that does not show average CT emission lifetimes decreasing as the wavelength increases from 475 to 550 nm. Second, its average emission lifetime in the CT region is 2.30 ± 0.20 ns (see Table 2). In contrast the average CT emission lifetime ($\langle\tau^{525}\rangle$ in Table 2) for the other five HPs that also lack electron traps is 1.06 ± 0.15 ns. HP **9** has a similar base sequence to HPs **1**−**3** and as expected by comparison with them has a similar emission spectrum (see Figure 2) and emission quantum yield (see Table 1). We have no explanation for the anomalous CT lifetime behavior of HP **9**, except to note that it has three Ts at its 5′-end flanking $U^{PE}$. Perhaps end fraying of the 5′-end T is responsible in some way for the anomalously long average CT emission lifetime of HP **9** compared to HPs **1**−**5**.

In addition to average emission lifetime components and amplitudes over both the dual wavelength and CT emission ranges for each HP, Table 2 also presents overall average lifetimes $\langle\tau\rangle$ and $\langle\tau^{525}\rangle$ in each emission range for each HP. In the dual wavelength range $\langle\tau\rangle$ is a simple amplitude weighted average of average lifetime components. In the CT emission range, however, the decrease of average CT emission lifetime with the wavelength increase shown in Figure 3 for HPs **1**−**8**, means that HP comparisons for these HPs have to be made at the same wavelength. Table 2, therefore, presents the lifetime at 525 nm from the linear least squares fit to average lifetime vs energy as this characteristic average CT emission lifetime, $\langle\tau^{525}\rangle$, for HP comparisons. As discussed above for individual wavelength emission kinetics measurements, the wavelength averaged results in Table 2 also show that eight HPs have large amplitude (generally ca. 0.5−0.7) ultrashort (ca. 0.1 ns) emission decays due to oxidative quenching of the pyrenyl $^1(\pi,\pi^*)$ state. In contrast, the shortest decay components in the CT emission region (generally ca. 0.3 ns) are all longer than the shortest decay components in the dual wavelength region.

HP **6**, however, is unique, because there is no evidence of the pyrenyl $^1(\pi,\pi^*)$ state at all either in its emission kinetics or in its emission spectrum (see Figure 2). Thus, the pyrenyl $^1(\pi,\pi^*)$ state of HP **6** appears to be completely quenched in less than 0.1 ns. Recall from Table 1 that HP **6** has an $U^F$ trap adjacent to $U^{PE}$ on the 5′-side. In fact HP **7** with a $U^{Br}$ trap adjacent to $U^{PE}$ also on the 5′-side is not too different from **6**. HP **7** shows only minimal amounts of pyrenyl $^1(\pi,\pi^*)$ state emission features in Figure 2 and very short (0.08 ns) pyrenyl quenching kinetics of very large amplitude (0.75) only in the 380−400 nm range. The other HP with $U^X$ traps is **8**. However, in **8** two Ts intervene in the 5′-direction between $U^{PE}$ and the $U^{Br}$ trap. The consequences of separating $U^{Br}$ from $U^{PE}$ are dramatic in two ways. First the average CT emission lifetime ($\langle\tau^{525}\rangle$) for **8** increases to 2.52 ns from 2.07 and 2.10 ns, respectively, for HPs **6** and **7**. Second, **8** has the largest emission quantum yield ($1.21 \times 10^{-2}$) of all nine HPs. Recall from Table 1 that the range of emission quantum yields for HPs **1**−**3** and **9** (that both lack electron traps and also have nearly pure CT emission spectra) is only $(0.14-0.27) \times 10^{-2}$.

More detailed emission quantum yield comparisons among HPs that also account for lifetime differences are even more revealing. HPs **1**−**3** have no traps and an average CT emission lifetime of 1.03 ± 0.16 ns; their average CT emission quantum yield is $(0.18 \pm 0.05) \times 10^{-2}$. However, HPs **6** and **7** with $U^X$ traps adjacent to $U^{PE}$ have an average CT emission lifetime of 2.09 ± 0.15 ns and an average CT emission quantum yield of $(0.84 \pm 0.20) \times 10^{-2}$. Thus, while the average CT lifetime increased 2-fold for the two HPs with traps compared to HPs **1**−**3**, their emission quantum yields increased even more, 2.8−4.7 times. Admittedly positioning electron traps immediately adjacent to $U^{PE}$ is not likely to be the best strategy for producing the longest-lived CS products. Thus, the lifetime and quantum yield results for HP **8** with two Ts separating the $U^{Br}$ trap and $U^{PE}$ are particularly significant. HPs **8** and **9** have similar average CT lifetimes, respectively, 2.52 and 2.30 ns (both ±0.20 ns). However, HP **9** lacking an electron trap has an emission quantum yield of only $0.27 \times 10^{-2}$, while HP **8** has a yield of $1.21 \times 10^{-2}$, a 4.5-fold increase. Thus, compared to HPs lacking traps, it is reasonable to conclude that HPs with electron traps in the 5′-direction on the same strand as $U^{PE}$ show enhanced CT emission quantum yields in excess of that expected based on comparison of average CT emission lifetimes.

## Conclusions

Eight HPs (all except **9**) showed linear correlations of their average CT emission lifetimes with the energy of the measured emission: higher energy emissions had longer average lifetimes (slower CR rates). This behavior cannot be due to a single $Py^{\bullet+}/dU^{\bullet-}$ CT state conformer for each HP. Rather, multiple conformations of CT states must exist for each HP solution. A similar argument holds as the reason that fitting the CT emission kinetics for all nine HPs at all wavelengths required three exponential lifetimes. Note that the minimum energy range spanned by the $Py^{\bullet+}/dU^{\bullet-}$ CT conformations with varying lifetimes is 0.4 eV. This is not unreasonable as a range of energy variation among $Py^{\bullet+}/dU^{\bullet-}$ CT states in a polar solvent.[28,30] The energy content of these CT states is also large (2.2−2.6 eV). Thus, their CRs are well into the inverted ET region as likely total (i.e., nuclear plus solvent) reorganization energies are 0.9 eV for nearest-neighbor CS and CR in DNA,[41] 0.8 eV for CS in cyclophane-bridged porphyrin-quinone systems in polar and nonpolar solvents,[42] and 0.6 ± 0.1 eV for nearest-neighbor hole injection in acridine-intercalated DNA.[43] Plots of ln $k_{ET}$ vs $\Delta G°$ for a family of ET reactions with rates $k_{ET}$ are known to be roughly quadratic over a large free energy range, but over a small free energy range well into the inverted region, they also appear linear.[44−47] In fact plotting average CT emission lifetimes $\langle\tau\rangle$ for HPs **1**−**8** as ln k, where $k = 1/\langle\tau\rangle$, vs emission energy produces linear fits to the data that are as good as those shown in Figure 3. This is not of itself a proof of CR behavior, but it is consistent with the above explanation of multiple conformations of CT states for the observed wavelength dependence of the average CT emission lifetime in HPs **1**−**8**.

The fact that HPs **1**−**5** lacking $U^X$ traps show an average CT lifetime, $\langle\tau\rangle$,[525] of 1.06 ± 0.15 ns indicates good reproducibility for this measurement whether same-strand Ts adjacent to the $U^{PE}$ electron source are present in both the 5′- and 3′-directions, present only in the 5′-direction, or even absent in both directions. In this context, the 2.30 ns average CT lifetime of HP **9** is anomalous as discussed above. In contrast to HPs **1**−**5** and **9**, however, all three HPs (**6**−**8**) with $U^X$ electron traps on the same strand as $U^{PE}$ have both an average CT lifetime in the 2.1−2.5 ns range and enhanced CT emission quantum yield (in excess of that expected based on relative CT lifetimes). The combination of these two differences for HPs **6**−**8** compared to all six other HPs strongly suggests that CS-2 type electron injection is occurring in $U^{PE}$ labeled HPs in addition to CS-1 type injection within $U^{PE}$ itself. This conclusion is further supported by the increase in pyrenyl $^1(\pi,\pi^*)$ emission features (see Figure 2) and in total emission quantum yield (see HPs **4** and **5** compared to HPs **1**−**3** in Table 1) that is seen as same strand Ts flanking $U^{PE}$ are switched to the opposite strand. The

increased CT emission quantum yield in HPs **6**−**8** compared to HPs **1**−**3** likely results from CS-2 injected electrons migrating to uracil in $U^{PE}$ (i.e., $Py^{\bullet+}dU$) and thus indirectly forming the emissive $Py^{\bullet+}/dU^{\bullet-}$ CT state of $U^{PE}$. This latter conclusion appears reasonable as excess electron hopping toward $Py^{\bullet+}dU$ is favored by Coulombic attraction. Finally, while this study presents compelling circumstantial evidence to support its conclusions, additional studies in this area would help cement its conclusions.

**Acknowledgment.** T.L.N. thanks the donors of the Petroleum Research Fund, administered by the American Chemical Society, for support of this research and Professor Nicholas E. Geacintov for helpful discussions.

**Supporting Information Available:** Text detailing the DNA HP analysis, HP concentration determination, UV−vis spectral determination (Figure 1S, HPs **2**−**4**, **6**, **7**, and **9**), CD spectra (Figure 2S, all HPs), emission quantum yield methods, emission lifetime methods, emission kinetics at individual wavelengths (Table 1S, from 380 to 550 nm for all HPs). This material is available free of charge via the Internet at http://pubs.acs.org.

## References and Notes

(1) Schuster, G. B., Ed. *Long-Range Electron Transfer in DNA I*; Springer-Verlag: Berlin, 2004; Vol. 236, p 219.
(2) Schuster, G. B., Ed. *Long-Range Electron Transfer in DNA II*; Springer-Verlag: Berlin, 2004; Vol. 237, p 244.
(3) Steenken, S. *Chem. Rev.* **1989**, *89*, 503−520.
(4) Steenken, S.; Telo, J. P.; Novais, H. M.; Candeis, L. P. *J. Am. Chem. Soc.* **1992**, *114*, 4701−4709.
(5) Steenken, S. *Free Radical Res. Commun.* **1992**, *16*, 349−379.
(6) Razskazovskii, Y.; Swarts, S. G.; Falcone, J. M.; Taylor, C.; Sevilla, M. D. *J. Phys. Chem. B* **1997**, *101*, 1460−1467.
(7) Messer, A.; Carpenter, K.; Forzley, K.; Buchanan, J.; Yang, S.; Razskazovskii, Y.; Cai, Z.; Sevilla, M. D. *J. Phys. Chem. B* **2000**, *104*, 1128−1136.
(8) Cai, Z.; Xifeng, L.; Sevilla, M. D. *J. Phys. Chem. B* **2002**, *106*, 2755−2762.
(9) Giese, B.; Carl, B.; Carl, T.; Carell, T.; Behrens, C.; Hennecke, U.; Shiemann, O.; Feresin, E. *Angew. Chem.* **2004**, *116*, 1884−1887.
(10) Ito, T.; Rokita, S. E. *Angew. Chem., Int. Ed.* **2004**, *43*, 1839−1842.
(11) Breeger, S.; Hennecke, U.; Carell, T. *J. Am. Chem. Soc.* **2004**, *126*, 1302−1303.
(12) Haas, C.; Kraling, K.; Cichon, M. K.; Rahe, N.; Carell, T. *Angew. Chem.* **2004**, *116*, 1878−1880.
(13) Behrens, C.; Burgdorf, L. T.; Schwogler, A.; Carell, T. *Angew. Chem., Int. Ed.* **2002**, *41*, 1763−1766.
(14) Cichon, M. K.; Haas, C.; Grolle, F.; Mees, A.; Carell, T. *J. Am. Chem. Soc.* **2002**, *124*, 13984−13985.
(15) Schwogler, A.; Burgdorf, L. T.; Carell, T. *Angew. Chem., Int. Ed.* **2000**, *39*, 3918−3920.
(16) Behrens, C.; Cichon, M. K.; Grolle, F.; Hennecke, U.; Carell, T. *Top. Curr. Chem.* **2004**, *236*, 187−204.
(17) Lewis, F. D.; Liu, X.; Wu, Y.; Miller, S. E.; Wasielewski, M. R.; Letsinger, R. L.; Sanishvili, R.; Joacimiak, A.; Tereshko, V.; Egli, M. *J. Am. Chem. Soc.* **1999**, *121*, 9905−9906.
(18) Lewis, F. D.; Liu, X.; Miller, S. E.; Hayes, R. T.; Wasielewski, M. R. *J. Am. Chem. Soc.* **2002**, *124*, 11280−11281.
(19) Lewis, F. D.; Wu, Y.; Liu, X. *J. Am. Chem. Soc.* **2002**, *124*, 12165−12173.
(20) Ito, T.; Rokita, S. E. *J. Am. Chem. Soc.* **2003**, *125*, 11480−11481.
(21) Wagenknecht, H.-A. *Curr. Org. Chem.* **2004**, *8*, 251−266.
(22) Rist, M.; Amann, N.; Wagenknecht, H.-A. *Org. Chem.—Eur. J.* **2003**, 2498−2504.
(23) Amann, N.; Pandurski, E.; Fiebig, T.; Wagenknecht, H.-A. *Angew. Chem., Int. Ed. Engl.* **2002**, *41*, 2978−2980.
(24) Amann, N.; Pandurski, E.; Fiebig, T.; Wagenknecht, H.-A. *Chem.—Eur. J.* **2002**, *8*, 4877−4883.
(25) Netzel, T. L.; Nafisi, K.; Headrick, J.; Eaton, B. E. *J. Phys. Chem.* **1995**, *99*, 17948−17955.
(26) Netzel, T. L.; Zhao, M.; Nafisi, K.; Headrick, J.; Sigman, M. S.; Eaton, B. E. *J. Am. Chem. Soc.* **1995**, *117*, 9119−9128.
(27) Korshun, V. A.; Manasova, E. V.; Balakin, K. V.; Prokhorenko, I. A.; Buchatskii, A. G.; Berlin, Y. A. *Rus. J. Bioorg. Chem.* **1996**, *22*, 807−809.
(28) Kerr, C. E.; Mitchell, C. D.; Headrick, J.; Eaton, B. E.; Netzel, T. L. *J. Phys. Chem. B* **2000**, *104*, 1637−1650.
(29) Kerr, C. E.; Mitchell, C. D.; Ying, Y.-M.; Eaton, B. E.; Netzel, T. L. *J. Phys. Chem. B* **2000**, *104*, 2166−2175.
(30) Mitchell, C. D.; Netzel, T. L. *J. Phys. Chem. B* **2000**, *104*, 125−136.
(31) Raytchev, M.; Mayer, E.; Amann, N.; Wagenknecht, H.-A.; Fiebig, T. *Chem. Phys. Chem.* **2004**, *5*, 706−712.
(32) Eckstein, J. W.; Hastings, J. W.; Ghisla, S. *Biochemistry* **1993**, *32*, 404−411.
(33) Li, X.; Sanche, L.; Sevilla, M. D. *J. Phys. Chem. A* **2002**, *106*, 11248−11253.
(34) Creutz, C.; Chou, M.; Netzel, T. L.; Okumura, M.; Sutin, N. *J. Am. Chem. Soc.* **1980**, *102*, 1309−1319.
(35) Duncan, D. C.; Netzel, T. L.; Hill, C. L. *Inorg. Chem.* **1995**, *34*, 4640−4646.
(36) Lakowicz, J. R. *Principles of Fluorescence Spectroscopy*; Plenum Press: New York, 1986; p 496.
(37) Moody, E. M.; Bevilacqua, P. C. *J. Am. Chem. Soc.* **2003**, *125*, 16285−16293.
(38) Moody, E. M.; Feerrar, J.; Bevilacqua, P. C. *Biochemistry* **2004**, *43*, 7992−7998.
(39) HPs **1**, **2**, **3**, **5**, and **9** were made first and have a G:A wobble loop-closing base pair. Initially, we thought that excess electrons might readily hop among pyrimidines in DNA, and we did not want them to hop onto a loop closing C and then into the tetra-T loop. Thus we used a G:A loop-closing base pair at first. After seeing that the average CT emission lifetime for **1**, **2**, **3** and **5** was essentially the same. It was clear that this worry was unfounded. We, therefore, felt comfortable using exclusively Watson−Crick base pairs in our second set of HPs (**4**, **6**, **7**, and **8**) and changed to a G:C loop-closing base pair in them. After the fact we carefully compared $T_m$ values, CD spectra, emission spectra, and average CT emission lifetimes for HPs with both types of closing base pairs. Based on this analysis and on review of published DNA and RNA loop structures, we conclude that $U^{PE}$-substituted HP structures and the excited-state dynamics of $U^{PE}$ in them are independent of the choice of G:A or G:C as a loop-closing base pair for the tetra-T DNA loop used in all nine of the duplexes studied in this paper. However, this is unlikely to be generally true for other DNA loops and is also unlikely to be true for most RNA loops.
(40) *HyperChem Professional*, Beta 1 Release 7.51 for Windows; Hypercube, Inc.: Gainesville, FL, 2003.
(41) Lewis, F. D.; Kalgutkar, R. S.; Wu, Y.; Liu, X.; Liu, J.; Hayes, R. T.; Miller, S. E.; Wasielewski, M. R. *J. Am. Chem. Soc.* **2000**, *122*, 12346−12351.
(42) Haberle, T.; Hirsch, J.; Pollinger, F.; Heitele, H.; Michel-Beyerle, M. E.; Anders, C.; Dohling, A.; Krieger, C.; Ruckemann, A.; Staab, H. A. *J. Phys. Chem.* **1996**, *100*, 18269.
(43) Davis, W. B.; Hess, S.; Naydenova, I.; Haselsberger, R.; Ogrodnik, A.; Newton, M.; Michel-Beyerle, M. E. *J. Am. Chem. Soc.* **2002**, *124*, 2422−2423.
(44) Siders, P.; Marcus, R. A. *J. Am. Chem. Soc.* **1981**, *103*, 748−752.
(45) Siders, P.; Marcus, R. A. *J. Am. Chem. Soc.* **1981**, *103*, 741−747.
(46) Marcus, R. A.; Siders, P. *J. Phys. Chem.* **1982**, *86*, 622−630.
(47) Mines, G. A.; Bjerrum, M. J.; Hill, M. G.; Casimiro, D. R.; Chang, I.-J.; Winkler, J. R.; Gray, H. B. *J. Am. Chem. Soc.* **1996**, *118*, 1961−1965.